Increased hemodynamic pulsatility in the cerebral microcirculation during parabolic flight-induced microgravity: A computational investigation

Stefania Scarsoglio [a,*], Matteo Fois [a], Luca Ridolfi [b]

[a] *Department of Mechanical and Aerospace Engineering, Politecnico di Torino, Corso Duca degli Abruzzi 24, Turin, 10129, Italy*
[b] *Department of Environmental, Land and Infrastructure Engineering, Politecnico di Torino, Corso Duca degli Abruzzi 24, Turin, 10129, Italy*

ABSTRACT

Ground-based spaceflight analogs play a crucial role to understand and predict cardiovascular alterations during microgravity in a controlled and affordable way. Despite their extensive use in recent years, cerebral hemodynamics in microgravity remains poorly understood, multifaceted, and definitive data are still missing, due to the limited number and different duration of experiments, the individual variability, and the intrinsic difficulty in obtaining direct clinical measures. However, there is growing evidence that hemodynamic changes are among the underlying causes of neurological dysfunctions, such as the Spaceflight Associated Neuro-ocular Syndrome (SANS). We proposed to investigate the cerebral hemodynamics during supine posture parabolic flight by means of a validated computational approach, combining a 0D-1D central-systemic cardiovascular model together with a 0D cerebrovascular model. Present findings showed that, although with over- and under-shoots in the transition from one gravitational environment to the other, beat-averaged pressure and flow rate steady state values did not greatly vary between 0g and 1g due to the cerebral autoregulation. On the contrary, in microgravity there was an augmented hemodynamic pulsatility which increased towards the deep cerebral microcirculation. The greater pulsatility, inducing a higher variability of maximum and minimum values reached within each beat, was here observed for the first time also for important cerebral markers, such as the intracranial pressure, the cerebrospinal fluid circulation, and the cerebral blood flow. The proposed approach offers novel insights on how hemodynamic alterations, such as cerebral hypoperfusions and intracranial pressure fluctuations, can contribute to explain neurovestibular dysfunctions emerging during short-term exposure to 0g, including the onset of nausea, SANS and cognitive fatigue.

1. Introduction

Long-term human spaceflight induces a number of cardiovascular alterations - such as fluid shift from lower to upper body, reduced exercise capacity, blood volume reduction, and cardiac atrophy - leading to cardiovascular deconditioning, that is the adaptation of the cardiovascular system to a less demanding environment [1–4]. Beside well known cardiovascular changes, cerebral circulation during microgravity is poorly understood. In fact, discrepancies and incongruent results from previous studies have not led to a firm understanding of cerebral hemodynamics in microgravity [5]. However, most reported neurological symptoms occurring after exposure to microgravity could be due to alterations in cerebral hemodynamics. Moreover, there is growing evidence that cerebral hemodynamic changes are among the main drivers and underlying causes of the Spaceflight Associated Neuro-ocular

Syndrome (SANS), classified today as one of the major risks for the human space exploration [6–8].

In this context, the use of ground-based analogs - such as bed-rest studies, dry immersions, and parabolic flights - is fundamental to understand in a controlled, cheap and affordable way, the underlying physiological mechanisms that are altered in cerebral hemodynamics during microgravity [5]. While bed-rest studies and dry immersions allow gravity unloading - the first by directing the gravity vector to the chest-back body axis and the second by substituting the gravity vector with the water hydrostatic gradient - parabolic flight is the only ground-based analog reproducing actual microgravity, although for few tens of seconds, by means of a free fall condition similar to that occurring on the International Space Station [9]. In fact, parabolic flight consists of a parabolic trajectory, performed 20–30 times for each experimental campaign, at the apex of which the condition of almost complete 0g is

reached. This 0g phase is preceded and followed by hypergravity conditions (1.8g), with each phase, including the transients from one gravitational state to another, lasting about 20 s.

Literature investigating cerebral hemodynamics and autoregulation has made extensive use of ground-based analogs in recent years. Some studies focused on how middle cerebral artery flow velocity changes during parabolic flight, discovering an important role of vascular resistance [10,11] and a link between cerebral hypoperfusion and orthostatic intolerance [12]. Marshall et al. [13], exploiting for the first time a magnetic resonance imaging technique, found a decrease in total arterial blood flow from baseline for different angles of bed-rest head down tilt. Following the seminal works by Ogoh et al. [14] and Lawley et al. [15], focus has been mainly devoted to provide estimates and surrogate measures of beat-averaged intracranial pressure and cerebral blood flow through different spaceflight analogs [5]. Furthermore, oxygenation studies [16,17] and neuropsychological tests [18] revealed that simulated 0g can enhance executive functioning and differently affect automatic and voluntary orienting of visuospatial attention.

The emerging picture is that microgravity-induced alterations of hemodynamics at the brain level are multifaceted and definitive data are missing. This gap is partially owing to the limited sample size of experiments, the individual variability, the different duration and functioning of the analogs [5]. Moreover, there is an intrinsic difficulty in obtaining direct and local clinical measures: currently adopted techniques usually fail in capturing the cerebral microvasculature hemodynamics. Even in 1g at resting conditions, transcranial Doppler ultrasonography [19] and 4D flow magnetic resonance imaging [20] can hardly be used beyond the circle of Willis and cannot give insights into the deep cerebral circulation. Most of the literature is in fact limited to beat-averaged measurements or estimates of intracranial pressure [5, 15], middle cerebral artery flow velocity [10,11], cerebral blood flow [14], and oxygenation [16,17]. To the best of our knowledge, information on the distal and venous-capillary circulation in terms of pressures and flow rates is lacking, and therefore understanding how proximal-to-distal hemodynamic patterns change in 0g is missing. Moreover, since all existing measures are beat-averaged, to date it is not possible to measure how the hemodynamic pulsatility and intrabeat variability change in 0g with respect to 1g, and whether they differently vary from the proximal to the distal circulation.

In this work, we aim to shed light on these gaps by studying the cerebral hemodynamics during parabolic flight-induced microgravity through a computational approach. This latter combines a 0D-1D model of the central-systemic circulation - recently validated [21,22] and used to investigate the cardiovascular response during parabolic [23] and long-term space flights [24] - together with a 0D model of the cerebrovascular circulation, already exploited to inquire into cardiac arrhythmias and heart rate variability effects on the cerebral hemodynamics [25–28]. With respect to our previous studies, which focused on the central hemodynamics and cardiac performance during parabolic flight [23] and on the cerebral hemodynamics in different pathological conditions [25–27], we here combine for the first time the two aspects by investigating the cerebral microcirculation response to parabolic flight-induced microgravity. The cerebrovascular model describes, in terms of pressures and flow rates, the cerebral circulation starting from the proximal inlet at the internal carotid artery level, passing through the large arteries of the circle of Willis, up to the distal circulation to reach the capillary-venous circulation. We considered the supine posture and focused on the left internal carotid artery - middle cerebral artery (ICA-MCA) pattern, which is representative of the proximal-to-distal pathway. The model allowed us to obtain continuous time-series, beat-averaged and pulsatile values of the whole cerebral circulation, in particular the distal-capillary pressures and flow rates which today are difficult to be measured in 0g. The present approach was able to shed light on the changes of the physiological proximal-to-distal cerebral circulation induced by microgravity, thus offering novel insights on how hemodynamic alterations, such as

cerebral hypoperfusions, intracranial pressure and cerebrospinal fluid (CSF) fluctuations, can contribute to explain neurovestibular dysfunctions - such as onset of nausea, visual impairment and cognitive fatigue - emerging during short-term exposure to 0g.

2. Methods

The main features of the central-systemic cardiovascular and cerebrovascular models are sketched in Fig. 1 and briefly described in the following. Governing equations, parameter setting, and numerical aspects are provided in the Supplementary Material, while further details, including modeling validation and applications, can be found in Refs. [23,25].
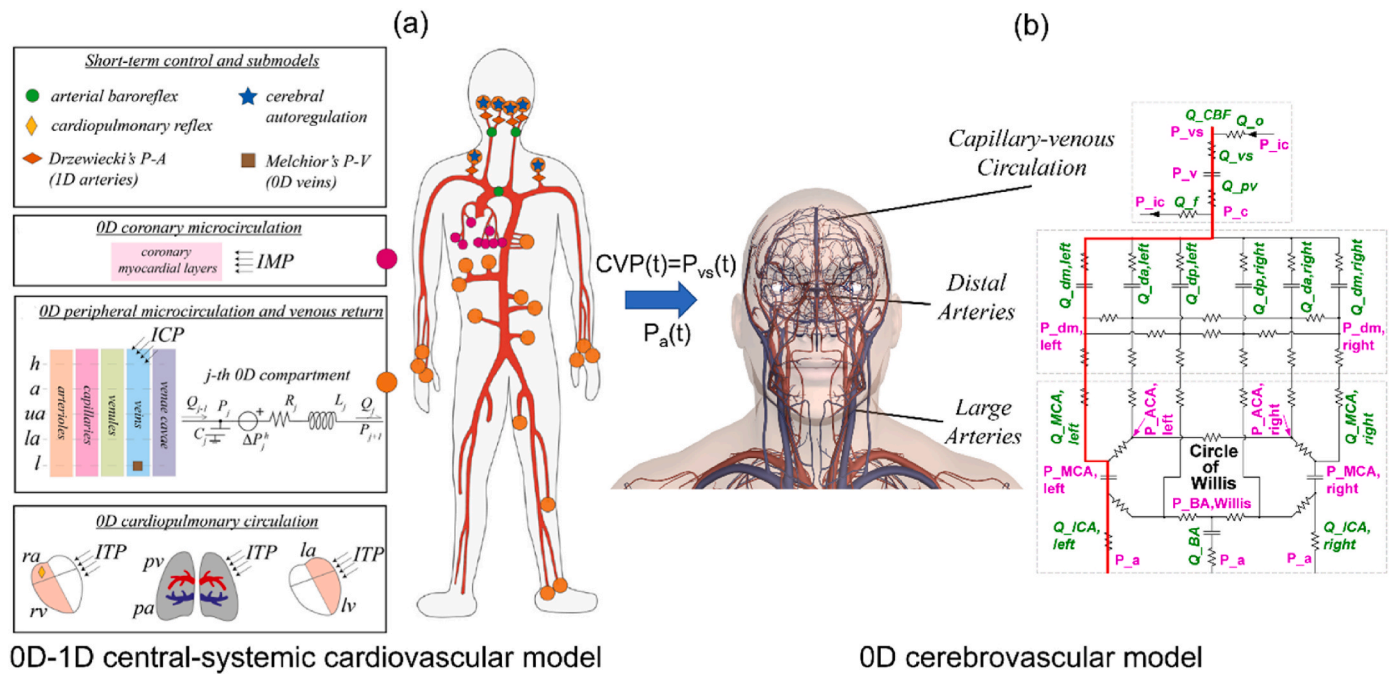
2.1. 0D-1D central-systemic cardiovascular model

The central-systemic cardiovascular model is multiscale (0D-1D) and closed-loop, with a 1D description of the arterial tree and a 0D lumped parameterization of the peripheral microcirculation, the venous return, and the cardiopulmonary circulation. A schematic representation of the central-systemic cardiovascular model is reported in Fig. 1a. Blood motion through 1D systemic arteries is governed by the axisymmetric form of the Navier-Stokes equations for mass and momentum balance, expressed in terms of flow rate and vessel cross-sectional area, where the gravity contribution is directly included through the Stevino's law, considering the orientation of the vessel with respect to the body axis and the horizontal reference. A constitutive non-linear equation, linking pressure and vessel area and accounting for viscoelastic properties, completes the differential system. The 0D side of the model includes lumped arteriolar, capillary, venular and venous RLC compartments organized into five body regions, i.e., head, arms, upper and lower abdomen, and legs, together with two inferior and one superior venae cavae compartments. The electrical components of the RLC analog are able to suitably reproduce the diffusive (resistance, R), inertial (inertance, L), and distensibility/contractility (compliance, C, or elastance, E) features of each cardiovascular region. The cardiopulmonary circulation includes 0D time-varying elastances for the four cardiac chambers, non-ideal diodes models of the heart valves, along with an arterial and a venous RC pulmonary compartment. The model also accounts for the action of specific extravascular pressures, such as the intramyocardial and intrathoracic pressures, and is equipped with short-term regulation mechanisms, that is baroreflex, cardiopulmonary reflex, and cerebral autoregulation models.

Full details of the governing equations and model parameters, as well as modeling validation, are offered elsewhere [23] and synthesized in the Supplementary Material. By solving the 0D-1D cardiovascular model, the resulting central aortic pressure, P_a, and the central venous pressure, CVP (that is, the right atrial pressure), were then used as forcing inputs for the forthcoming cerebrovascular model.

2.2. 0D cerebrovascular model

The open-loop 0D cerebral model, schematically sketched in Fig. 1b, required two time-series inputs: the central aortic pressure, P_a, and the dural sinus pressure, P_{vs}. The first was directly obtained from the 0D-1D central-systemic cardiovascular model. For the dural sinus pressure, in the supine posture the jugular veins are widely open and P_{vs} can be approximated through CVP [15,29], thus we here assumed $P_{vs} = $ CVP, with CVP as taken from the 0D-1D central-systemic model. The 0D cerebrovascular model describes the arterial and venous cerebral circulation, by including the circle of Willis and six regional districts perfused by the six main cerebral arteries, which are independently controlled by autoregulation and CO_2 reactivity. The microcirculation vascular beds communicate via distal inter-regional anastomoses. The cerebral venous circulation is defined by two-element Windkessel modeling, while the cerebrospinal fluid (CSF) circulation, originated at the level of cerebral

Fig. 1. Scheme of the combined computational models (R: resistance, C: compliance, L: inertance, Q: flow rate, P: pressure, V: volume, A: vessel area). (a) 0D-1D central-systemic cardiovascular model. The red network on the right represents 1D arteries, while left panels summarize the matching with the 0D compartments: short-term regulation models; coronary microvascular compartments (IMP: intramyocardial pressure); peripheral microcirculation and venous return (h: head, a: arms, ua: upper abdomen, la: lower abdomen, l: legs), with a sketch of the j-th compartment electric RLC analog; cardiopulmonary circulation (where ra, rv, la and lv are right atrium and ventricle, left atrium and ventricle, respectively, p_a and p_v are pulmonary arteries and veins, ITP is the intrathoracic pressure). (b) 0D cerebrovascular model. The left ICA-MCA pathway is highlighted in red and composed by: central aortic pressure, P_a (forcing inlet, together with the dural sinus pressure, P_{vs}, of the cerebrovascular model), left internal carotid artery flow rate, $Q_{ICA, left}$, left middle cerebral artery pressure $P_{MCA, left}$, left middle cerebral artery flow rate, $Q_{MCA, left}$, left middle distal pressure, $P_{dm,left}$, left middle distal flow rate, $Q_{dm,left}$, capillary pressure, P_c, proximal venous flow rate, Q_{pv}, intracranial pressure, P_{ic}, total cerebral blood flow, Q_{CBF}. (For interpretation of the references to color in this figure legend, the reader is referred to the Web version of this article.)

capillaries and absorbed at the dural venous sinus level, is modeled through resistive components. The intracranial pressure is computed by applying the mass preservation and assuming a monoexponential pressure-volume relationship for the craniospinal system. A network of time-varying RC circuits describes the cerebral circulation from the large arteries level up to the peripheral and capillary regions. The cerebral circulation is expressed in terms of pressure, volume, and flow rate, and can be divided into three principal regions: large arteries, distal arterial circulation, and capillary-venous circulation. The model was validated in physiological and pathological conditions up to the middle cerebral circulation [25,28], since definitive clinical data in the microvasculature are still missing. Being able to reproduce several different pathological conditions characterized by heterogeneity in cerebrovascular hemodynamics, the 0D cerebral model was exploited to investigate the effects of cardiac arrhythmias [25–27] and heart rate variability [28] on the deep cerebral circulation.

The left internal carotid artery - middle cerebral artery (ICA-MCA) vascular pathway was focused upon (see the red path in Fig. 1b), in terms of pressure (P) and blood flow rate (Q), as representative of the hemodynamics from large arteries to the capillary-venous circulation: P_a and $Q_{ICA, left}$ (proximal signals at the inlet), $P_{MCA, left}$ and $Q_{MCA, left}$ (representative of the large cerebral arteries), $P_{dm,left}$ and $Q_{dm,left}$ (representative of the distal cerebral circulation), P_c and Q_{pv} (representative of the capillary-venous cerebral circulation), P_{ic} and Q_{CBF} (intracranial pressure and total cerebral blood flow). CSF circulation, in terms of formation and absorption flow rates (Q_f and Q_o, respectively), was as well investigated.

Details of the differential equations, model parameters, autoregulation mechanisms, and validation can be found elsewhere [25], and are recalled in the Supplementary Material.

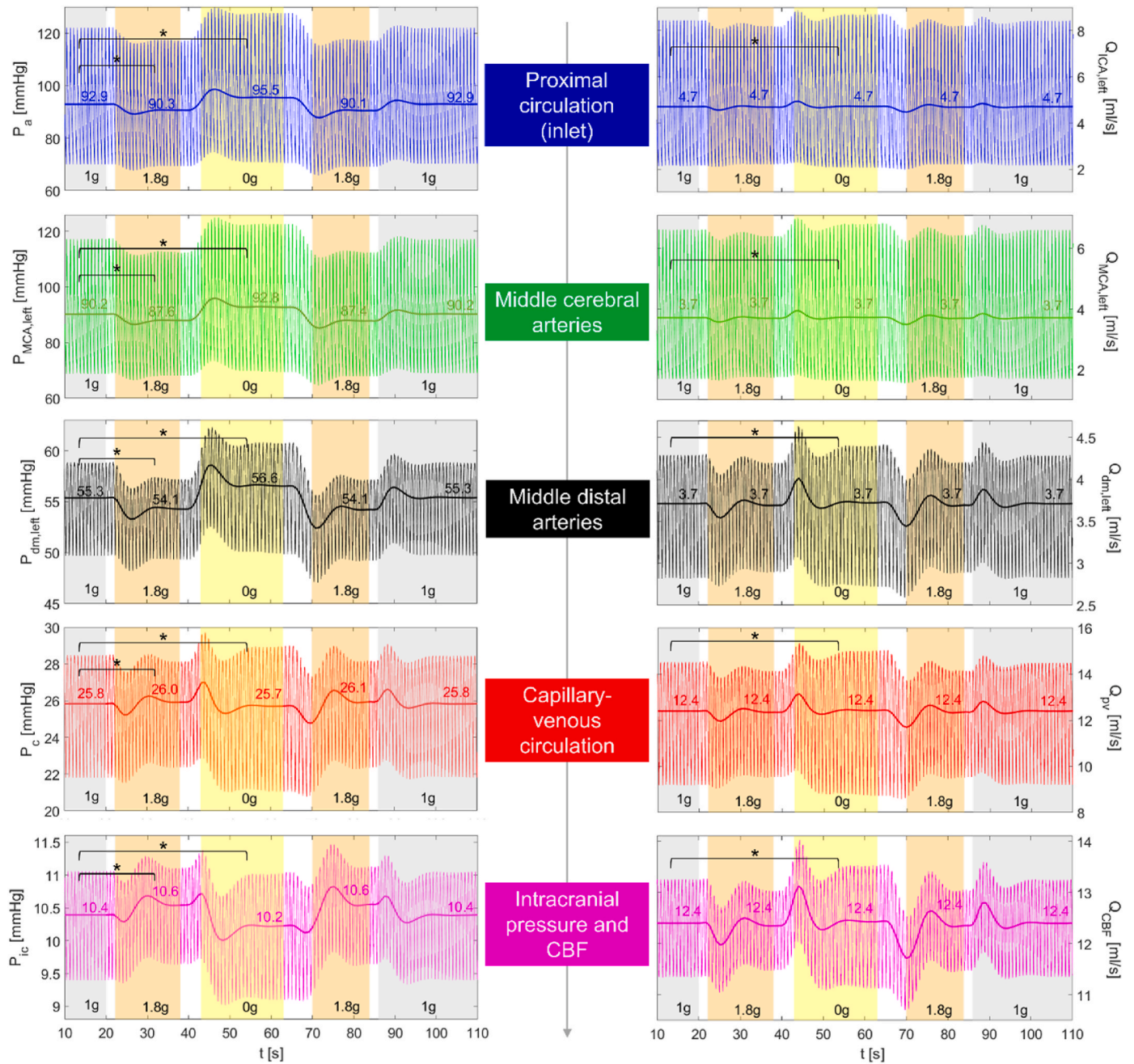### 2.3. Parabolic flight simulation

A standard parabolic flight profile was simulated, as adopted in Ref. [23]. After the initial 1g phase, an hypergravity phase (1.8g) lasting about 20 s followed. Then, at the apex of the parabola, the microgravity (0g) condition was reached and maintained for approximately 20 s, before a subsequent hypergravity phase (1.8g) again of about 20 s was faced. The session ended with restoration of the 1g condition. Fast transitions between each phase lasted few seconds (1g–1.8g: about 2 s; 1.8g–0g: 5–7 s). The time-varying gravity load was expressed as a cosinusoidal function, whose details are offered in Ref. [23].

3. Results

The 0D-1D central-systemic cardiovascular model here used to force the 0D cerebrovascular model was already validated and exploited to study the central hemodynamic and cardiac performance during parabolic flight [23]. For the supine posture, it was found that stroke volume (SV) increased in 0g and decreased in 1.8g, while heart rate (HR) decreased in 0g and increased in 1.8g. Moreover, no evident variation of the oxygen demand–supply balance and mean central aortic pressure emerged [23].

We first show in Fig. 2 an overview of the cerebral hemodynamics during parabolic flight, by reporting pairs of analyzed pressure (P) and flow rate (Q) signals along the left ICA-MCA pattern (P_a and $Q_{ICA, left}$; $P_{MCA, left}$ and $Q_{MCA, left}$; $P_{dm,left}$ and $Q_{dm,left}$; P_c and Q_{pv}; P_{ic} and Q_{CBF}), each representative of a cerebral vascular region. Fig. 2 also displays beat-averaged timeseries (thick curves) of P and Q signals, as well as their steady state values for each flight phase computed averaging the last 10 s of each phase [23]. Over- and under-shoots for all the P and Q signals were present at the beginning of each phase, as a result of the

Fig. 2. Overview of the pressure, P (left), and flow rate, Q (right), signals during parabolic flight. From top to bottom (proximal to distal circulation): P_a, $Q_{ICA, left}$, $P_{MCA, left}$, $Q_{MCA, left}$, $P_{dm,left}$, $Q_{dm,left}$, P_c, Q_{pv}, P_{ic}, and Q_{CBF}. Thick curves show beat-averaged time-series, while their steady state values for each flight phase (displayed as colored numbers) were computed averaging the last 10 s of each phase. Asterisks and black lines indicate significant (p-value<0.05) parameter differences for 1g–1.8g and 1g–0g comparisons.

abrupt transition from one gravitational environment to the other. Overall, pressure steady state values experienced slight (within 3%) but in general significant variations during the different phases of flight with respect to 1g (Paired-Sample *t*-Test for steady state pressure values: p-value<0.001 for 1g–1.8g and 1g–0g comparisons), while negligible and in general less significant variations were found for flow rate steady state values (Paired-Sample *t*-Test for steady state flow rate values: p-value<0.03 for 1g–0g; not significant for 1g–1.8g). Fig. 2 reveals that over- and under-shoots of the beat-averaged series, as well as maximum and minimum values reached by the continuous signals, were not of the same magnitude in the different vascular districts.

To better quantify the observed proximal-to-distal differences, in Fig. 3 we compared beat-averaged values of P (panel a) and Q (panel b)

signals (normalized with respect to the corresponding 1g beat-averaged values), and pulsatile values per beat of pressure ($\Delta P = P_{max} - P_{min}$, panel c) and flow rate ($\Delta Q = Q_{max} - Q_{min}$, panel d) (normalized with respect to the corresponding 1g pulsatile values), along the left ICA-MCA pattern during parabolic flight. Starting with beat-averaged P values (Fig. 3a), a protective behavior was observed for the distal-capillary regions: here, over- and under-shoots always extinguished earlier in time than in the proximal districts. Overall, this implies that the highest variations were within ±4% in the distal-capillary area, against ±6% in the proximal area, therefore in the deep circulation the cerebral autoregulation damped out sudden changes induced at proximal level. Moreover, in 0g, up to the distal level $\overline{P}/\overline{P}_{1g} > 1$ was found, while in the capillary-venous regions $\overline{P}/\overline{P}_{1g} < 1$. The contrary held in hypergravity
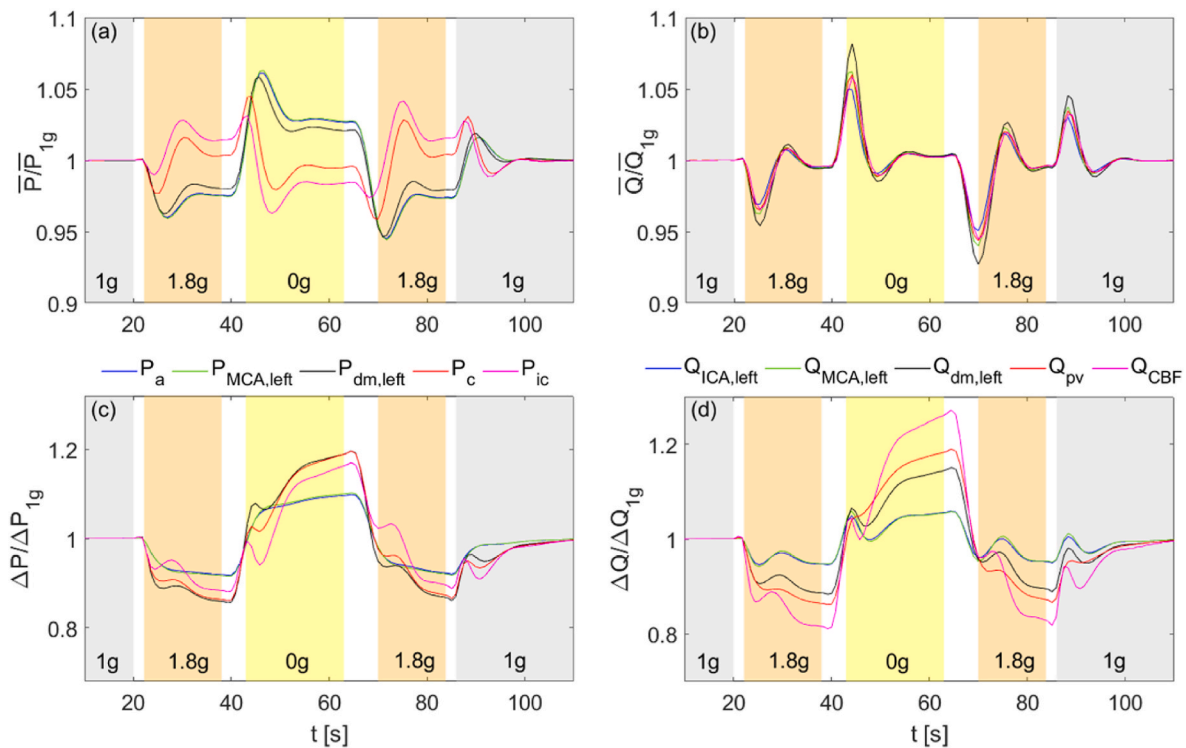
Fig. 3. Beat-averaged and pulsatile values for pressure and flow rate signals along the ICA-MCA pathway (P_a and $Q_{ICA, left}$ (blue curves) almost overlap with $P_{MCA, left}$ and $Q_{MCA, left}$ (green curves), respectively). Ratio between: (a) mean pressure per beat and mean pressure per beat at 1g, $\overline{P}/\overline{P}_{1g}$; (b) mean flow rate per beat and mean flow rate per beat at 1g, $\overline{Q}/\overline{Q}_{1g}$; (c) pulsatile pressure per beat and pulsatile pressure per beat at 1g, $\Delta P/\Delta P_{1g}$; (d) pulsatile flow rate per beat and pulsatile flow rate per beat at 1g, $\Delta Q/\Delta Q_{1g}$. (For interpretation of the references to color in this figure legend, the reader is referred to the Web version of this article.)

phases. Beat-averaged Q values (Fig. 3b) instead did not present any time lag, within each phase $\overline{Q}/\overline{Q}_{1g}$ proximal-to-distal variations were always either all <1 or all >1, and all variations (including over- and under-shoots) were within ±8% (the most stressed was on average the distal district).

As already stated, steady state variations (in 1.8g and 0g, with respect to 1g) were quite limited for P and negligible for Q, for all the vascular regions analyzed. In particular, the intracranial pressure, P_{ic}, showed a very slight decrease during short-term microgravity (1g: 10.4 mmHg; 0g: 10.2 mmHg), which is in agreement with [5,15], who found that P_{ic} in short-term exposure to microgravity remained basically unchanged. Our findings confirm that in supine posture P_{ic} remained at mildly-elevated levels not only in 0g but in all the phases of parabolic flight, even with a slight increase (+2%) in the hypergravity phase. In supine condition, differently to the upright posture, not only the 0g phase prevented the normal lowering of P_{ic} [5], but this happened also during the 1.8g phase, and therefore P_{ic} was constant and high throughout the parabolic flight. The slight variation between 1g and 0g of the mean P_{ic} at steady state was comparable to the ones observed in the upstream cerebral compartments (<3%) and was mainly due to the mechanisms of cerebral autoregulation. The latter acted by directly regulating the flow rates (in terms of time-varying distal compliances and resistances), guaranteeing a constant average perfusion and therefore negligible average flow rate variations between 1g and 0g. Pressures were not directly ruled by the cerebral autoregulation, but maintaining a constant mean perfusion in turn implied that the mean pressure variations between 1g and 0g were slight.

To investigate the difference between maximum and minimum values reached within each beat for the P and Q signals, pulsatile values ΔP and ΔQ were reported (normalized with respect to the corresponding 1g pulsatile values) in Fig. 3c and d, respectively. Differently to beat-averaged values, pulsatile values of all P and Q variables largely varied during the 1.8g and 0g phases and did not usually reach steady state

values at the end of each phase. In particular, during 0g, pulsatile values increased by up to 20–30% in the distal-capillary circulation, while they did not exceed 5–10% in the large arteries region: in this regard, the protective (P signals) or maintenance (Q signals) effects, which were seen for the beat-averaged values, were here lost. Pulsatile values variations (positive in 0g, negative in 1.8g) increased in the proximal-to-distal direction with respect to the 1g phase. There was, therefore, a strongly amplifying effect of the pulsatile values in the deep cerebral circulation due to the complex interplay between the different mechanical and structural features of the cerebral circulation, expressed by a combination of resistance and compliance components of different magnitude [26]. Similarly to a system of in series and parallel springs - where the damping of an imposed oscillation is lengthened by the combination of the stiffness of the springs -, here when proximal pulsatile signals propagated into the cerebral vessel network, the distal and capillary regions remained altered for longer. As a consequence, the temporal inertia of the system increases towards the microvasculature and this in turn enhanced (in module) the variation of the pulsatile values introduced at the proximal level.

Moreover, for both P and Q signals, a contraction of the pulsatile values (negative variations) was observed during 1.8g, while an amplification (positive variations) was found during 0g, with respect to the 1g phase. This behavior was induced by the central hemodynamics, since pulse pressure at the central aortic level, namely ΔP_a, is approximately proportional to the stroke volume, SV [30]: as previously mentioned, in 1.8g, HR increased and SV decreased, thus reducing the pulsatility of P_a and consequently $Q_{ICA, left}$. On the contrary, in 0g, HR decreased and SV increased, thus the pulsatility of P_a and $Q_{ICA, left}$ increased [23]. Then, in the deep cerebral circulation, the reduced proximal pulsatility was further damped in 1.8g, while the increased proximal pulsatility was further amplified in 0g, due to the above mentioned enhancement (in absolute terms) of the variations of pulsatile values towards the distal regions.

Fig. 4 shows the behavior of the CSF circulation, in terms of formation and absorption flow rates, Q_f and Q_o, respectively. Being Q_f driven by the pressure drop ($P_c - P_{ic}$), while Q_o by the pressure drop ($P_{ic} - P_{vs}$), CSF circulation is intrinsically related to the P_{ic} behavior. Recent measures found an increase of brain ventricular volume and subarachnoid space - that is where the CSF is formed - and a widespread spatial redistribution of CSF after long-term spaceflight [31–34]. The larger volumes observed in astronauts developing SANS suggest that altered CSF and fluid accumulation in brain ventricles may play a role in the onset of SANS [31,32]. Our beat-averaged Q_f results (Fig. 4a, blue curve) highlighted in early 0g a CSF formation flow rate peak, which was rapidly damped thanks to the cerebral autoregulation. CSF absorption rate (beat-averaged Q_o, red curve in Fig. 4a) showed that: (i) the matching between formation and absorption rates present in 1g was instead impaired during parabolic flight, also at the steady states of 1.8g and 0g phases; (ii) at least for short-term 0g, CSF accumulation was prevented by a higher CSF absorption rate. Similarly to what previously observed for the distal variables, also for the CSF circulation, the hemodynamic pulsatility (Fig. 4b) was higher in 0g, with a more evident increase (+20%) for the formation flow rate, Q_f.

In the end, we focused on the comparison between the cerebral perfusion pressure, CPP, defined as $P_a - P_{ic}$, and the cerebral blood flow, Q_{CBF}, Fig. 5. CPP is the driver of the blood flow into the brain, providing oxygen and nutrients, and the primary determinant and estimate of Q_{CBF} [14]. By comparing beat-averaged values of CPP and Q_{CBF} in Fig. 5a, transient over- and under-shoots were in general more marked for CPP than Q_{CBF}, thus resulting in higher (in absolute terms) variations at steady state for CPP than Q_{CBF}. In fact, in 0g at steady state CPP slightly and significantly increased (Paired-Sample *t*-Test for steady state values: p-value<0.001 for 1g–1.8g and 1g–0g), in agreement with [14], while barely significant variations (Paired-Sample *t*-Test for steady state values: p-value = 0.4 for 1g–1.8g; p-value = 0.03 for 1g–0g) emerged for Q_{CBF}. By considering pulsatile values of CPP and Q_{CBF} (Fig. 5b), the higher Q_{CBF} pusatility during 0g was underestimated by CPP, and the reduced Q_{CBF} pulsatility during 1.8g was underestimated (in module) by CPP.

Therefore, CPP remained a good proxy of Q_{CBF} during parabolic flight, however it did not take into account the effects of vasodilatation/constriction due to cerebral autoregulation mechanisms, particularly important in the distal circulation. These mechanisms caused the distal vascular resistance to vary especially in transients between one gravitational environment and another, such as to guarantee a constant Q_{CBF} mean value at steady state in all the phases, which was not true for CPP.

4. Discussion and conclusions

By combining a 0D-1D model of the central-systemic circulation together with a 0D model of the cerebrovascular circulation, in this work we focused on the cerebral hemodynamics during a typical parabola of a supine posture parabolic flight session. In fact, roughly 20 s of 1g horizontal flight were sufficient to fully recover the hemodynamic reference baseline condition (that is, steady state 1g supine), at least within the processes described by our model. Therefore, if the parabolas of a parabolic flight session are separated by at least 20 s, all the parabolas share the same hemodynamic alterations. If, on the other hand, the parabolas are spaced out by less than 20 s, we expect that the first phase of each parabola (that is, the 1.8g phase) may show more marked over- and under-shoots than presented above. However, the duration of about 20 s of the 1.8g phase should allow the full resorption of these peak values and the achievement of steady state 1.8g values equal in all parabolas. Therefore, if the duration and succession of the parabola does not change (about 20 s 1.8g, 20 s 0g, 20 s 1.8g) we do not expect any significant accumulation effect leading to an increasing/decreasing hemodynamic trend even if the parabolas are closer together, since each phase (1.8g or 0g) lasts a sufficient time (about 20 s) to restore the corresponding hemodynamic steady state. Finally, an interval of less than 20 s between one parabola and another can be hardly achieved in terms of flight maneuvers, thus the results shown are representative, from a hemodynamic point of view, of a generic parabola within a parabolic flight session.

We found that beat-averaged hemodynamic values showed limited variations throughout the different flight phases. In fact, beat-averaged variations at steady state (with respect to 1g) were all significant and within 3% for pressures, while were negligible and less significant for flow rates. Present findings regarding mean Q_{CBF} values are in line with Ogoh et al. [14], who found that dynamic cerebral autoregulation counteracts acute variations in the cerebral blood perfusion and volume during parabolic flight. Our results, in addition to being in line with those of Ogoh et al. [14] in terms of mean Q_{CBF} values, are also consistent with those of [10,11] in showing that the mean $Q_{MCA,\ left}$ at steady state does not vary significantly between 1g and 0g. Klein et al. first [10] observed that middle cerebral artery velocity remained unchanged during 0g compared to 1g. Then, they measured that middle cerebral artery velocity first decreased and subsequently increased during 0g, explaining this behavior through the activation of cerebrovascular resistance in order to avoid hyperperfusion of the brain [11]. Our findings also showed that constant steady state values of beat-averaged flow rates seem to be ruled by the interplay between cerebrovascular vasodilatation and vasoconstriction, which guarantees an adequate average cerebral perfusion in all the steady state flight phases. Transient over- and under-shoots of beat-averaged values between one phase and another were as well modest (in absolute terms): for pressure signals, a reduction (from 6% to 4%) was observed from proximal to distal circulation, while a moderate increase (from 4% to
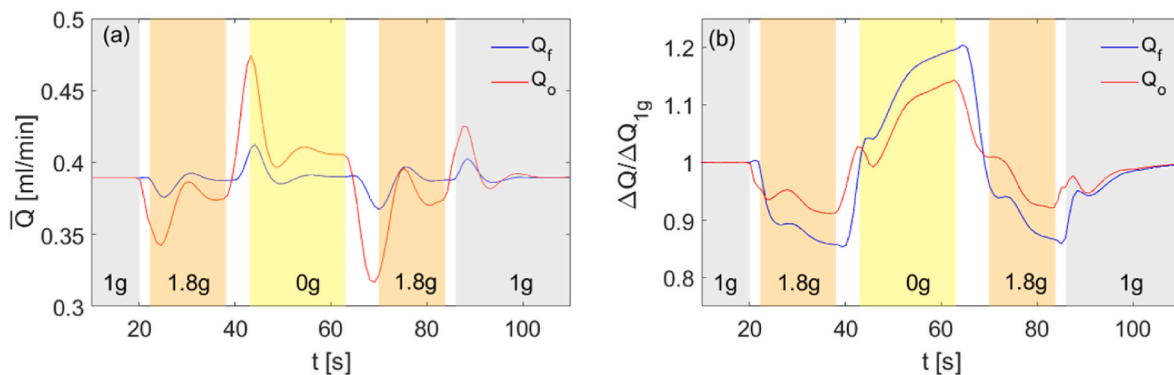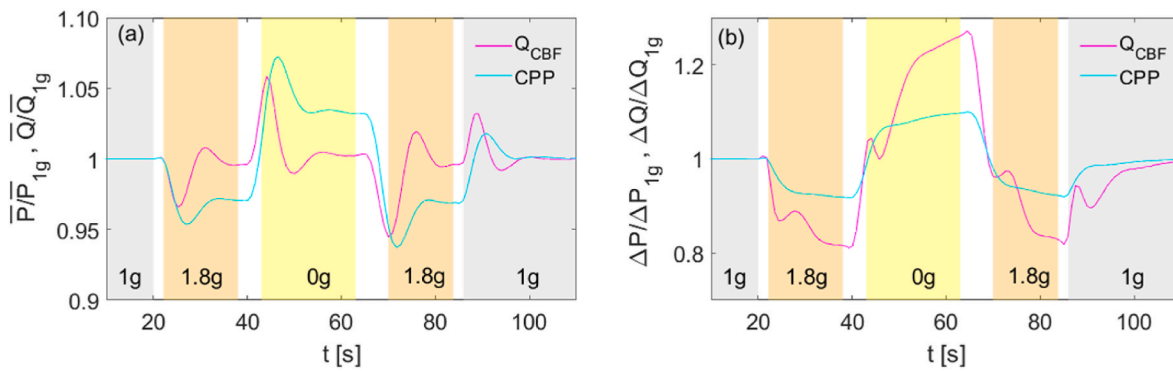

Fig. 4. Cerebrospinal fluid (CSF) circulation: formation (Q_f, blue curves) and absorption (Q_o, red curves) flow rates. (a) Mean flow rates per beat, $\overline{Q}$ [ml/min]. (b) Ratio between pulsatile flow rate per beat and pulsatile flow rate per beat at 1g, $\Delta Q/\Delta Q_{1g}$. (For interpretation of the references to color in this figure legend, the reader is referred to the Web version of this article.)

Fig. 5. Beat-averaged and pulsatile values for the cerebral perfusion pressure, CPP, and the total cerebral blood flow, Q_{CBF}. Ratio between: (a) mean CPP per beat and mean CPP per beat at 1g, $\overline{P}/\overline{P}_{1g}$; mean Q_{CBF} per beat and mean Q_{CBF} per beat at 1g, $\overline{Q}/\overline{Q}_{1g}$; (b) pulsatile CPP per beat and pulsatile CPP per beat at 1g, $\Delta P/\Delta P_{1g}$; pulsatile Q_{CBF} per beat and pulsatile Q_{CBF} per beat at 1g, $\Delta Q/\Delta Q_{1g}$.

8%) was found in the same proximal-to-distal direction for flow rates.

To corroborate the fundamental role of the cerebral autoregulation in maintaining physiological perfusion and pressure levels during parabolic flight, we increased the latency time, $\tau_{aut} = 20$ s at baseline - which regulates the response time of the distal compliances and resistances - by a factor of 2, 5, and 10, see Eq. (S35) in the Supplementary Material. We briefly recall that by increasing τ_{aut}, the autoregulation system was slower in its response, that is autoregulation effects within the parabolic flight were reduced. We focused on beat-averaged values of microcirculation variables (normalized with respect to beat-averaged values at 1g), by choosing P_c, $Q_{dm,left}$, and Q_f, as representative of the distal-capillary circulation behavior, see Fig. 6. We observed that for all the variables considered, over- and under-shoots occurring in between two gravitational environments were much more pronounced in amplitude and delayed in time, as τ_{aut} increased. Furthermore, at $\tau_{aut} = 200$ s, which represents a response latency approximately twice the duration of the parabolic flight, during the steady state of all flight phases full recovery of the 1g average perfusion was no longer restored (see $Q_{dm,left}$ and Q_f, panels 6b and 6c, red curves). The behavior highlighted in Fig. 6 confirms that the control of the over- and under-shoots and then the steady state recovery were at large the result of the action of the cerebral autoregulation system.

Differently from the beat-averaged behavior, pulsatile values ΔP and ΔQ, which are markers of hemodynamic variability, experienced instead large variations even with perfectly functioning cerebral autoregulation. To the best of our knowledge, pulsatile values have never been reported in literature and represent a piece of novelty of the present study. In particular, there was an increased variability during 0g (with respect to

1g) in the distal-capillary regions: up to +20% for the CSF circulation, distal-capillary and intracranial pressures, up to +30% for the venous flow rate and cerebral blood flow. The higher variability implies that short-term microgravity makes the deep cerebral circulation more exposed to very high or low values compared to the beat-averaged values, leading to an overall higher risk of mechanical stress and potential cerebrovascular injury. In fact, in resting 1g condition, increased intracranial and MCA pulsatility have been associated to cerebral small vessel disease [35] and cognitive impairment [36].

Finally, the comparison between CPP and Q_{CBF} showed that CPP remained a good proxy of Q_{CBF}. However, CPP, not directly taking into account the cerebral autoregulation, overestimated the beat-averaged steady state variations while underestimated the pulsatility of Q_{CBF} in 0g. In this regard, we recall that low Q_{CBF} values can be predictive of the onset of nausea [14]. It is worth mentioning that a reduction of Q_{CBF} was also correlated to chronic fatigue syndrome [37,38], thus the transiently impaired Q_{CBF} activation and regulation, as evidenced by the occurrence of overshoots and undershoots as well as the increased pulsatility, may be here linked to cognitive fatigue symptoms. Q_{CBF} monitoring (in terms of average values and pulsatility) is therefore particularly important also for neurovestibular implications during parabolic and space flights [14].

The present work had some limiting aspects. First, there was a one-way coupling from the 0D-1D central-systemic cardiovascular model to the 0D cerebral model, since no cerebral circulation feedbacks returned to the 0D-1D cardiovascular model. Second, the cerebrovascular model assumed a perfectly functioning cerebral autoregulation throughout the parabolic flight, even if autonomic dysfunction, in terms of increased response latency, was discussed. In the end, the central-
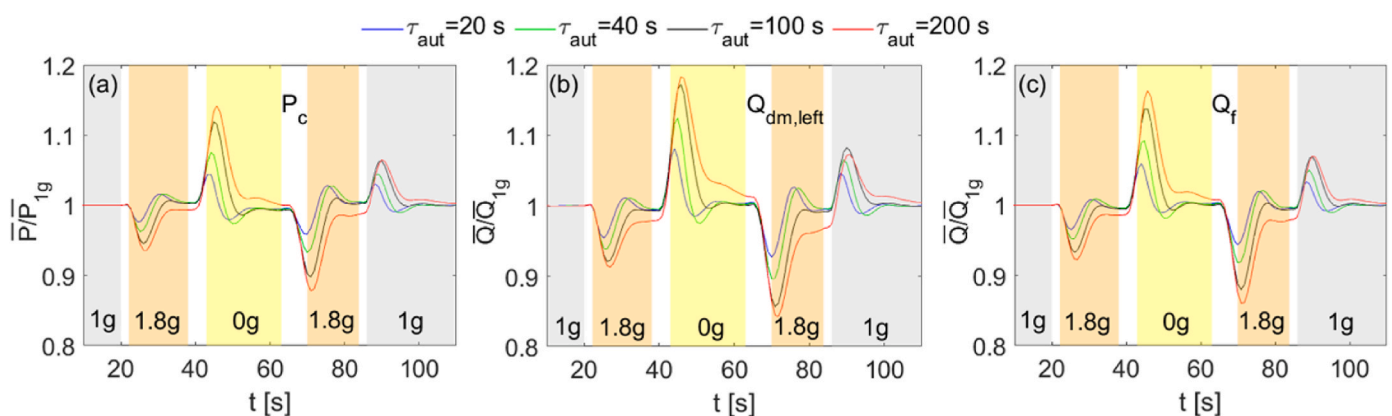
Fig. 6. Role of the cerebral autoregulation. Effects of the latency time, τ_{aut}, on the microcirculation: (a) capillary pressure, P_c; (b) left middle distal flow rate, $Q_{dm,left}$; (c) CSF formation flow rate, Q_f. $\tau_{aut} = 20$ s (baseline, blue curves), $\tau_{aut} = 40$ s (green curves), $\tau_{aut} = 100$ s (black curves), $\tau_{aut} = 200$ s (red curves). (For interpretation of the references to color in this figure legend, the reader is referred to the Web version of this article.)

systemic 0D-1D model lacked of muscular intervention mechanisms and metabolic regulation of blood pressure and flow, which can play a role especially in the 1.8g stressing condition.

In conclusion, the model is a powerful and predictive tool in highlighting novel insights into the cerebral hemodynamics during parabolic flight as well as in different spaceflight scenarios to be explored in future works, such as the sudden hypergravity condition (up to 3g) during orbital re-entry after prolonged exposure to 0g. In the present study, the patterns of Q_{CBF} and P_{ic} were among the most important, being Q_{CBF} the index of global cerebral perfusion and P_{ic} one of the main determinant of intraocular pressure (IOP) and thus possibly one of the main hemodynamic driver of the SANS [6–8]. Although steady state beat-averaged values of both Q_{CBF} and P_{ic} did not vary between 1g and 0g, these two variables showed instead important increases in their pulsatile values (the highest among all those analyzed) during 0g. These results mean that the 0g phase on average does not alter Q_{CBF} and P_{ic} values compared to 1g, but exposes to a higher variability of maximum and minimum values reached within a beat. A high Q_{CBF} variability, which during anesthesia and surgery has been linked to post operative delirium and cognitive disorders [39,40], can have implications also for human health in space flight, holding the potential to promote cerebral hypoperfusions and cerebral microcirculation damage, especially during the prolonged exposure to 0g of long-term spaceflights. Analyzing pressure and flow rate pulsatile values, apart from beat-averaged values, can be a new precious key of reading to explain possible Q_{CBF} transient hypoperfusions - and the consequent onset of nausea and cognitive fatigue - as well as anomalous P_{ic} (and therefore IOP) fluctuations and transient CSF production/absorption flow rates mismatch - such as to induce visual impairment and consequently contribute to the SANS - emerging during short-term exposure to 0g.

Credit authors statement

S. S. and L. R. conceived and designed the research. S. S. performed the numerical simulations, drafted the manuscript and prepared the figures. All authors analyzed and interpreted the results, edited, reviewed and approved the final version of the manuscript.

Data availability statement

The raw data generated and analyzed during the current study will be made available from the corresponding author on reasonable request.

Declaration of competing interest

The authors declare that they have no known competing financial interests or personal relationships that could have appeared to influence the work reported in this paper.

Acknowledgment

References

[1] P. Norsk, Adaptation of the cardiovascular system to weightlessness: surprises, paradoxes and implications for deep space missions, Acta Physiol. 228 (2020), e13434, https://doi.org/10.1111/apha.13434.

[2] R.L. Hughson, A. Helm, M. Durante, Heart in space: effects of the extraterrestrial environment on the cardiovascular system, Nat. Rev. Cardiol. 15 (2018) 167–180, https://doi.org/10.1038/nrcardio.2017.157.

[3] H. Zhu, H. Wang, Z. Liu, Effects of real and simulated weightlessness on the cardiac and peripheral vascular function on humans: a review, Int. J. Occup. Med. Environ. Health 28 (2015) 793–802, https://doi.org/10.13075/ijomeh.1896.00301.

[4] H.C. Gunga, V. Weller von Ahlefeld, H.J. Appell Coriolano, A. Werner, U. Hoffmann, Cardiovascular System, Red Blood Cells, and Oxygen Transport in Microgravity, Springer, 2016, https://doi.org/10.1007/978-3-319-33226-0.

[5] J. Du, J. Cui, J. Yang, P. Wang, L. Zhang, B. Luo, B. Han, Alterations in cerebral hemodynamics during microgravity: a literature review, Med. Sci. Mon. 27 (2021), e928108, https://doi.org/10.12659/MSM.928108.

[6] A.G. Lee, T.H. Mader, C.R. Gibson, T.J. Brunstetter, W.J. Tarver, Space flight-associated neuro-ocular syndrome (sans), Eye 32 (7) (2018) 1164–1167, https://doi.org/10.1038/s41433-018-0070-y.

[7] A.G. Lee, T.H. Mader, C.R. Gibson, W. Tarver, P. Rabiei, R.F. Riascos, L. A. Galdamez, T. Brunstetter, Spaceflight associated neuro-ocular syndrome (sans) and the neuroophthalmologic effects of microgravity: a review and an update, npj Microgravity 6 (1) (2020) 7, https://doi.org/10.1038/s41526-020-0097-9.

[8] L.F. Zhang, A.R. Hargens, Spaceflight-induced intracranial hypertension and visual impairment: pathophysiology and countermeasures, Physiol. Rev. 98 (1) (2018) 59–87, https://doi.org/10.1152/physrev.00017.2016.

[9] A. Saveko, M. Bekreneva, I. Ponomarev, I. Zelenskaya, A. Riabova, T. Shigueva, V. Kitov, N. Abu Sheli, I. Nosikova, I. Rukavishnikov, D. Sayenko, E. Tomilovskaya, Impact of different ground-based microgravity models on human sensorimotor system, Front. Physiol. 14 (2023), 1085545, https://doi.org/10.3389/fphys.2023.1085545.

[10] T. Klein, P. Wollseiffen, M. Sanders, J. Claassen, H. Carnahan, V. Abeln, T. Vogt, H. K. Strüder, S. Schneider, The influence of microgravity on cerebral blood flow and electrocortical activity, Exp. Brain Res. 237 (4) (2019) 1057–1062, https://doi.org/10.1007/s00221-019-05490-6.

[11] T. Klein, M. Sanders, P. Wollseiffen, H. Carnahan, V. Abeln, C. Askew, J. Claassen, Transient cerebral blood flow responses during microgravity, Life Sci. Space Res. 25 (2020) 66–71, https://doi.org/10.1016/j.lssr.2020.03.003.

[12] J.M. Serrador, J.K. Shoemaker, T. Brown, M.S. Kassam, R. Bondar, T.T. Schlegel, Cerebral vasoconstriction precedes orthostatic intolerance after parabolic flight, Brain Res. Bull. 53 (1) (2000) 113–120, https://doi.org/10.1016/S0361-9230(00)00315-4.

[13] K. Marshall-Goebel, K. Ambarki, A. Eklund, J. Malm, E. Mulder, D. Gerlach, E. Bershad, J. Rittweger, Effects of short-term exposure to head-down tilt on cerebral hemodynamics: a prospective evaluation of a spaceflight analog using phase-contrast mri, J. Appl. Physiol. 120 (12) (2016) 1466–1473, https://doi.org/10.1152/japplphysiol.00841.2015.

[14] S. Ogoh, A. Hirasawa, P.B. Raven, T. Rebuffat, P. Denise, R. Lericollais, J. Sugawara, H. Normand, Effect of an acute increase in central blood volume on cerebral hemodynamics, Am. J. Physiol. - Reg. I. 309 (8) (2015) R902–R911, https://doi.org/10.1152/ajpregu.00137.2015.

[15] J.S. Lawley, L.G. Petersen, E.J. Howden, S. Sarma, W.K. Cornwell, R. Zhang, L. A. Whitworth, M.A. Williams, B.D. Levine, Effect of gravity and microgravity on intracranial pressure, J. Physiol. 595 (6) (2017) 2115–2127, https://doi.org/10.1113/JP273557.

[16] S. Mekari, R.J.L. Murphy, A.R.S. MacKinnon, Q. Hollohan, S.C. Macdougall, M. K. Courish, D.S. Kimmerly, H.F. Neyedli, The impact of a short-period head-down tilt on executive function in younger adults, Sci. Rep. 12 (1) (2022), 20888, https://doi.org/10.1038/s41598-022-25123-3.

[17] S. Schneider, V. Abeln, C.D. Askew, T. Vogt, U. Hoffmann, P. Denise, H.K. Strüder, Changes in cerebral oxygenation during parabolic flight, Eur. J. Appl. Physiol. 113 (6) (2013) 1617–1623, https://doi.org/10.1007/s00421-013-2588-9.

[18] A. Salatino, C. Iacono, R. Gammeri, S.T. Chiad`o, J. Lambert, D. Sulcova, A. Mouraux, M.S. George, D.R. Roberts, A. Berti, R. Ricci, Zero gravity induced by parabolic flight enhances automatic capture and weakens voluntary maintenance of visuospatial attention, npj Microgravity 7 (1) (2021) 29, https://doi.org/10.1038/s41526-021-00159-3.

[19] S. Purkayastha, F. Sorond, Transcranial Doppler ultrasound: technique and application, Semin. Neurol. 32 (4) (2012) 411–420, https://doi.org/10.1055/s-0032-1331812.

[20] T. Vikner, L. Nyberg, M. Holmgren, J. Malm, A. Eklund, A. W°ahlin, Characterizing pulsatility in distal cerebral arteries using 4D flow mri, J. Cerebr. Blood F. Met 40 (12) (2020) 2429–2440, https://doi.org/10.1177/0271678X19886667.

[21] M. Fois, S.V. Maule, M. Giudici, M. Valente, L. Ridolfi, S. Scarsoglio, Cardiovascular response to posture changes: multiscale modeling and in vivo validation during head-up tilt, Front. Physiol. 13 (2022), 826989, https://doi.org/10.3389/fphys.2022.826989.

[22] M. Fois, L. Ridolfi, S. Scarsoglio, Arterial wave dynamics preservation upon orthostatic stress: a modelling perspective, R. Soc. Open Sci. 10 (3) (2023), 221257, https://doi.org/10.1098/rsos.221257.

[23] M. Fois, L. Ridolfi, S. Scarsoglio, In silico study of the posture-dependent cardiovascular performance during parabolic flights, Acta Astronaut. 200 (2022) 435–447, https://doi.org/10.1016/j.actaastro.2022.08.018.

[24] C. Gallo, L. Ridolfi, S. Scarsoglio, Cardiovascular deconditioning during long-term spaceflight through multiscale modeling, npj Microgravity 6 (1) (2020) 27, https://doi.org/10.1038/s41526-020-00117-5.

[25] M. Anselmino, S. Scarsoglio, A. Saglietto, F. Gaita, L. Ridolfi, Transient cerebral hypoperfusion and hypertensive events during atrial fibrillation: a plausible mechanism for cognitive impairment, Sci. Rep. 6 (2016), 28635, https://doi.org/10.1038/srep28635.

[26] S. Scarsoglio, A. Saglietto, M. Anselmino, F. Gaita, L. Ridolfi, Alteration of cerebrovascular haemodynamic patterns due to atrial fibrillation: an in silico investigation, J. Roy. Soc. Interface 14 (129) (2017), 20170180, https://doi.org/10.1098/rsif.2017.0180.

[27] A. Saglietto, S. Scarsoglio, L. Ridolfi, F. Gaita, M. Anselmino, Higher ventricular rate during atrial fibrillation relates to increased cerebral hypoperfusions and hypertensive events, Sci. Rep. 9 (1) (2019) 3779, https://doi.org/10.1038/s41598-019-40445-5.

[28] S. Scarsoglio, L. Ridolfi, Different impact of heart rate variability in the deep cerebral and central hemodynamics at rest: an in silico investigation, Front. Neurosci. 15 (2021) 600574, https://doi.org/10.3389/fnins.2021.600574.

[29] M. Ursino, M. Giannessi, A model of cerebrovascular reactivity including the circle of willis and cortical anastomoses, Ann. Biomed. Eng. 38 (3) (2010) 955–974. https://doi.org/10.1007/s10439-010-9923-7.

[30] A.C. Guyton, J.E. Hall, Textbook of Medical Physiology, twelfth ed., Elsevier Saunders, Philadelphia, 2011.

[31] G. Barisano, F. Sepehrband, H.R. Collins, S. Jillings, B. Jeurissen, J.A. Taylor, C. Schoenmaekers, C. De Laet, I. Rukavishnikov, I. Nosikova, L. Litvinova, A. Rumshiskaya, J. Annen, J. Sijbers, S. Laureys, A. Van Ombergen, V. Petrovichev, V. Sinitsyn, E. Pechenkova, A. Grishin, P.z. Eulenburg, M. Law, S. Sunaert, P. M. Parizel, E. Tomilovskaya, D.R. Roberts, F.L. Wuyts, The effect of prolonged spaceflight on cerebrospinal fluid and perivascular spaces of astronauts and cosmonauts, P. Natl. Acad. Sci. USA 119 (17) (2022), e2120439119. https://10.1073/pnas.2120439119.

[32] N. Alperin, A.M. Bagci, C.J. Oliu, S.H. Lee, B.L. Lam, Role of cerebrospinal fluid in spaceflight-induced ocular changes and visual impairment in astronauts, Radiology 285 (3) (2017) 1063. https://10.1148/radiol.2017174039.

[33] S. Jillings, A. Van Ombergen, E. Tomilovskaya, A. Rumshiskaya, L. Litvinova, I. Nosikova, E. Pechenkova, I. Rukavishnikov, I.B. Kozlovskaya, O. Manko, S. Danilichev, S. Sunaert, P.M. Parizel, V. Sinitsyn, V. Petrovichev, S. Laureys, P. Eulenburg, J. Sijbers, F.L. Wuyts, B. Jeurissen, Macro- and microstructural changes in cosmonauts' brains after longduration spaceflight, Sci. Adv. 6 (36) (2020), eaaz9488. https://10.1126/sciadv.aaz9488.

[34] A. Van Ombergen, S. Jillings, B. Jeurissen, E. Tomilovskaya, A. Rumshiskaya, L. Litvinova, I. Nosikova, E. Pechenkova, I. Rukavishnikov, O. Manko, S. Danylichev, R.M. Rühl, I.B. Kozlovskaya, S. Sunaert, P.M. Parizel, V. Sinitsyn, S. Laureys, J. Sijbers, P.Z. Eulenburg, F.L. Wuyts, Brain ventricular volume changes induced by long-duration spaceflight, P. Natl. Acad. Sci. USA 116 (21) (2019) 10531–10536. https://10.1073/pnas.1820354116.

[35] Y. Shi, M.J. Thrippleton, G.W. Blair, D.A. Dickie, I. Marshall, I. Hamilton, F. N. Doubal, F. Chappell, J.M. Wardlaw, Small vessel disease is associated with altered cerebrovascular pulsatility but not resting cerebral blood flow, J. Cerebr. Blood Flow Metabol. 40 (1) (2020) 85–99. https://10.1177/0271678X18803956.

[36] C.P. Chung, H.Y. Lee, P.C. Lin, P.N. Wang, Cerebral artery pulsatility is associated with cognitive impairment and predicts dementia in individuals with subjective memory decline or mild cognitive impairment, J. Alzheimers Dis. 60 (2) (2017) 625–632. https://10.3233/JAD-170349.

[37] B. Biswal, P. Kunwar, B.H. Natelson, Cerebral blood flow is reduced in chronic fatigue syndrome as assessed by arterial spin labeling, J. Neurol. Sci. 301 (1–2) (2011) 9–11, https://doi.org/10.1016/j.jns.2010.11.018.

[38] A.J. Ocon, Caught in the thickness of brain fog: exploring the cognitive symptoms of chronic fatigue syndrome, Front. Physiol. 4 (2013) 63, https://doi.org/10.3389/fphys.2013.00063.

[39] S. Deiner, J.H. Silverstein, Postoperative delirium and cognitive dysfunction, Br. J. Anaesth. 103 (Suppl 1) (2009) i41–i46, https://doi.org/10.1093/bja/aep291.

[40] C. Huang, J. Mårtensson, I. Gögenur, M.S. Asghar, Exploring postoperative cognitive dysfunction and delirium in noncardiac surgery using mri: a systematic review, Neural Plast. 1281657 (2018) 2018, https://doi.org/10.1155/2018/1281657.